applied sciences

MDPI

Article

Nonlinear Vibrations of Low Pressure Turbine Bladed Disks: Tests and Simulations

Umidjon Usmanov [1,*], Giuseppe Battiato [1], Christian Maria Firrone [1], Marta Conte [2], Emanuele Rosso [2] and Antonio Giuseppe D'Ettole [2]

[1] Department of Mechanical and Aerospace Engineering, Polytechnic University of Turin, 10129 Turin, Italy; giuseppe.battiato@polito.it (G.B.); christian.firrone@polito.it (C.M.F.)
[2] Avio Aero, 10040 Turin, Italy; marta.conte@avioaero.it (M.C.); emanuele.rosso@avioaero.it (E.R.)
* Correspondence: umidjon.usmanov@polito.it

Abstract: One of the most effective methods to limit the mechanical vibrations of bladed disks is the use of friction damping at mechanical joint interfaces. Unfortunately, dedicated tests to assess the impact of mistuning and the effectiveness of friction dampers are uncommon. This paper presents an original design of an academic demonstrator to perform an experimental analysis of the dynamic response of a tip-free bladed disk with under-platform dampers (UPDs), including an identification of intrinsic and contact mistuning introduced by the UPDs. The 48-blade disk was tested in a vacuum spinning rig by using permanent magnets. Vibration measurements were performed with the Blade Tip-Timing system. Tests were simulated using the Policontact tool, which predicted the average experimental nonlinear response in the presence of UPD, confirming the tool's ability to capture the general nonlinear dynamic behavior of the mistuned bladed disk. This study presents a novel approach combining experimental Blade Tip Timing (BTT) with numerical simulations using Policontact (ver. 3.0) software and a model update based on experimental evidence to validate nonlinear dynamic responses. It distinguishes between intrinsic and contact mistuning effects, providing new insights into their impact on bladed disk vibrations. Additionally, a comparison of aluminum and steel UPDs reveals that steel offers a 26% greater damping efficiency due to its higher density and preload, significantly improving vibration reduction.

Keywords: bladed-disk vibration; friction damper; underplatform damper; nominal mistuning; blade tip timing; rotating test rig

Citation: Usmanov, U.; Battiato, G.; Firrone, C.M.; Conte, M.; Rosso, E.; D'Ettole, A.G. Nonlinear Vibrations of Low Pressure Turbine Bladed Disks: Tests and Simulations. *Appl. Sci.* **2024**, *14*, 10597. https://doi.org/10.3390/app142210597

Academic Editor: Florent Ravelet

Received: 9 October 2024
Revised: 11 November 2024
Accepted: 12 November 2024
Published: 17 November 2024

1. Introduction

In modern engineering, the efficient operation of turbomachinery is crucial for numerous industrial processes, including power generation, aviation, water, oil and gas exploitation, and chemical processing. The performance of turbomachinery is vital for productivity, safety, and sustainability. Central to this machinery are complex interactions of forces, materials, and dynamic phenomena, with vibrations being a critical aspect. These vibrations, stemming from rotor unbalance, aerodynamic forces, mechanical resonance, and fluid–structure interactions, can range from benign to harmful. Understanding and mitigating these vibrations is essential to prevent accelerated wear, fatigue, and potential catastrophic failure, making it a key focus of research and engineering.

Friction damping devices are commonly employed in turbomachinery to minimize vibration amplitudes and improve the longevity and reliability of bladed disks. These dampers work by dissipating vibrational energy, thereby protecting the machinery from excessive wear and potential failure [1]. The study of the performance of dampers has attracted both academic and practical attention. Some techniques [2–7] have investigated the performance of so-called ring dampers to reduce vibration amplitude through energy dissipation at the friction contact in the rim interface. In particular, ref. [4] presented

a design of a new passive damper coupling the energy-dissipative mechanisms of dry friction and a piezoelectric shunting circuit for integrally bladed disks. Other studies [8,9] have focused on the impacts of a dissipative mechanism in reducing blade vibration. However, there is a study [10] that developed semi-active dry friction dampers which allow the control of the normal force for a reduction in steady-state vibration. Concerning conventional underplatform dampers, numerous studies [11–22] have been performed to study their dynamic properties and damping efficiency. Specifically, ref. [12] proposed a new numerical tool to analyze the dynamic behavior of bladed disk systems with UPDs. This tool utilizes time-marching algorithms to perform individual time domain simulations under the harmonic excitation of certain frequencies. Gao et al. [11] investigated the effect of frictional heat on the performance of UPDs. The results revealed a significant influence which may lead to a strong misprediction of the optimal centrifugal force and underestimation of the resonant peak in the presence of frictional heat. While some works have put a focus on the experimental or the numerical analysis of UPDs [14,19], others have performed both [13,15,18,20–22]. Botto et al. [19] presented a new approach to evaluate damper–blade interaction. This resulted in a more insightful and less uncertain experimental investigation of damper behavior. Ferhatoglu et al. [13] numerically and experimentally investigated the nonlinear response variability in turbine bladed disks coupled with UPDs. They proposed a method which is able to predict the experimentally measured variability range with numerically calculated limits. Li et al. [21] developed a blade vibration test system for capturing damping characteristic curves through frequency sweep excitation and damping-free vibration methods. Fantetti et al. [22] compared the experimental and numerical nonlinear dynamic responses of a bladed disk with UPD. As a result, the guidelines were proposed to enhance the nonlinear dynamic modeling approaches. On the other hand, there is a study by Denimal et al. [16] which tried to modify the geometric properties of UPD to improve the damping efficiency. This geometry was based on a conical shape, which prevented the pure rolling motion of the damper and ensured a high kinematic slip. The results revealed that this geometry has a high damping capacity and is more robust than conventional ones. Additionally, Li et al. explored the multiphase vortex-induced vibration (MVIV) in hydropower systems. They developed a fluid–structure coupling principle that provides new theoretical perspectives for understanding MVIV behaviors [17].

A comprehensive literature review revealed gaps in combining experimental and numerical methods to study the nonlinear vibration of bladed disks, particularly in relation to mistuning effects and material-specific UPD efficiency. This study presents several novel contributions to address these gaps:

- *Development of an academic demonstrator*: a 48-bladed disk scaled down from a 144-bladed design. This scaled disk allows for the efficient analysis of large bladed disk dynamics, which are challenging to handle at full size. The scaled model facilitates the repeatability of tests, saves time, and enables a comprehensive inspection of all underplatform dampers, making it a valuable tool for dynamic behavior analysis.
- *Combined experimental and numerical approach:* this work integrates experimental Blade Tip Timing (BTT) analysis with numerical simulations using Policontact software, allowing the accurate validation of the model with experimental data.
- *Mistuning analysis:* this study distinguishes between intrinsic (manufacturing) and contact (UPD-induced) mistuning, providing deeper insights into their individual effects on dynamic response.
- *Material-specific damping efficiency:* the comparison of aluminum and steel UPDs reveals that steel offers greater damping efficiency due to its higher density and preload.

In this context, the EU (European Union)-funded project AriAS (Advanced Research into Aeromechanical Solutions) [23] aimed at producing unprecedented ground experiments in the aeronautical engineering field to develop more reliable analytical tools, improving current methods employed by aircraft engine manufacturers to predict and prevent aeromechanical vibrations.

The study presented in this paper was developed within the AriAS project; it aims to investigate, both experimentally and numerically, the combined effects of intrinsic mistuning (mainly due to machining tolerance and assembly uncertainties) and under-platform dampers (UPDs) on the dynamic response of a dummy bladed disk. The bladed disk was designed by scaling the original 144-blade ARiAS test article (TA) to facilitate an experimental test campaign under controlled conditions using an academic test rig located at the AerMec laboratory for turbine and compressor components at Politecnico di Torino. Additionally, numerical forced response simulations, both with and without under-platform dampers, were performed in order to compare the numerical results with measurements and finally the assess limits and advantages of performing calculations when the cyclic symmetry properties of the nominal, ideally tuned, bladed-disk geometry are used. The comparison deals with the effects of natural mistuning on the dynamic response of the scaled TA, and how the same response is influenced by the friction nonlinearities due to UPDs.

2. Experiment

The experiment was performed on a purposely designed 48-blade scaled TA (Figure 1). The number of blades was defined in order to take into account the room available for the spinning test rig, the possibility to keep the cavity where the UPDs are positioned as close as possible to the original cavity, and, finally, the possibility to easily repeat multiple tests by removing and inserting all the blades and UPDs in a limited amount of time. The scaled bladed disk has been designed from the original one of the AriAS project (144 blades) by preserving the main geometrical features. In particular, the two TA disks supported the same blade and UPD geometry and materials; the same space between adjacent blades at the platform–shank region was preserved, since it is the location where the UPD is inserted; the same Inter-Blade Phase Angle (IBPA) for the excited nodal diameter modes of the original disk was used in order to measure the UPDs' damping effectiveness with the same platform kinematics. Therefore, the ratio between the number of blades of the reference disk and the modified one can be used to scale the nodal diameters under investigation. Specifically, ND8 related to the third modal family used in this work. The term "third modal family" refers to a set of natural frequencies where specific nodal diameter (ND) patterns emerge, with ND8 representing the mode with eight nodal diameters. The choice of this mode was motivated by the full-scale 144-blade disk's operational conditions, where it experiences resonance crossing with the ND8 mode during service. This selection allows our scaled model to replicate the relevant dynamic behavior observed in the full-scale disk. ND8 corresponds to the ND24 mode of the reference disk in order to have a common IBPA = 60°.

(**a**) (**b**) (**c**)

Figure 1. (**a**) ARIAS 48-blade disk assembly; (**b**) disk blade unit; (**c**) under-platform dampers. Scaled and re-designed version of 144-bladed disk assembly used in ARIAS project.

The smaller radius of the scaled test rig did not allow us to keep the same critical rotating speed at which resonance excitation occurs. For this reason, it was decided to firmly press the blade root against the disk slot by means of screws aligned along the radial direction. In this way, the friction damping at the blade root joint is prevented and the measured damping will be associated with the action of the material and UPDs only.

Post-processing, all the experimental data underwent a forced-response measurement for each blade as well as for critical frequency values by means of the Blade Tip Timing (BTT) system. The BTT system is employed to measure the vibration amplitude of each blade and monitor the disk speed by ensuring the proper positioning of sensors which are placed on the rig casing. Excitation was realized by means of permanent magnets, as in the reference disk, which are mounted on a static flange. Static magnets interact with rotating magnets mounted on the tip of each blade of the rotor.

Before proceeding with the rotating test, a non-rotating impact test was performed to identify the material damping and the resonant frequency associated with the ND8 mode shape.

As the next step, the blade is experimentally tested in static and rotating conditions. The experimental spinning rig features two protective cylindrical structures, shown in Figure 2a: an external (component n.2) and an internal one (component n.1). The bladed disk is secured to the rotating shaft within the internal structure using bolts. Two flanges are mounted to the inner ring: the lower flange holds the excitation system based on permanent magnets; the upper flange holds the measurement system based on laser sensors, according to a Blade Tip Timing (BTT) setup.

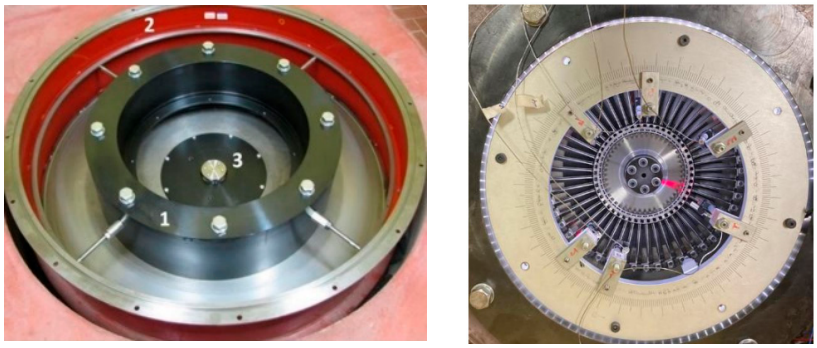

(**a**) (**b**)

Figure 2. (**a**) Vertical axis spinning test rig (top view); (**b**) bladed disk within spinning test rig.

2.1. Modal Hammer Testing

Initially, a hammer test is performed on the bladed disk without UPDs, which are already connected to the flange of the rotating shaft in the spinning rig (Figure 2b). Hammer test measurements are a non-destructive testing method commonly employed in engineering to understand the dynamic behavior of systems. During the test, a hammer equipped with a load cell at its tip is used to measure the impact force on the component being tested. The structure's recorded response to the impact allows us to determine Frequency Response Functions (FRFs). These data are crucial for understanding the structure's behavior in terms of natural frequencies and mode shapes if multiple output measurements are collected. In this study, the response of the bladed disk is recorded with a non-contact, optical (laser)-scanning measurement technique. The hammer testing method consists of the separate excitation of each blade with an impulse and measuring the corresponding response of the blades. The post-processing software allows users to convert the input force and output response via Fast Fourier Transform (FFT) into the frequency domain and the Frequency Response Function (FRF) is calculated based on input and output data. Several impacts are applied for the same measurement to collect multiple FRFs from different measurement target points; averages for each measurement point are calculated in order to minimize

random errors (three hits per target point). As an example, the measured data on the 38th blade are represented in Figure 3.

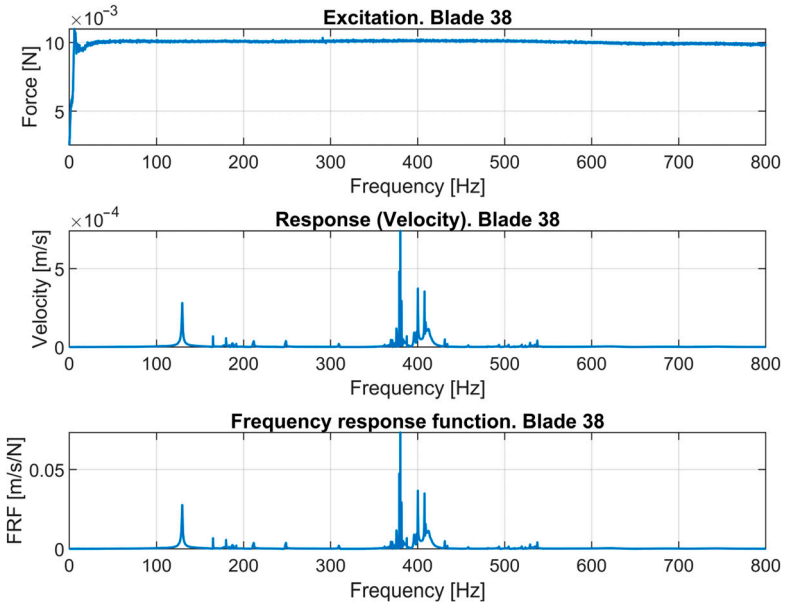

Figure 3. Excitation, response, and frequency response function measurements performed on 38th blade by hammer test.

Afterwards, the ND8 mode related to the third modal family is identified and the corresponding maximum response and corresponding critical frequency are plotted as a function of the blade number, as presented in Figure 4.

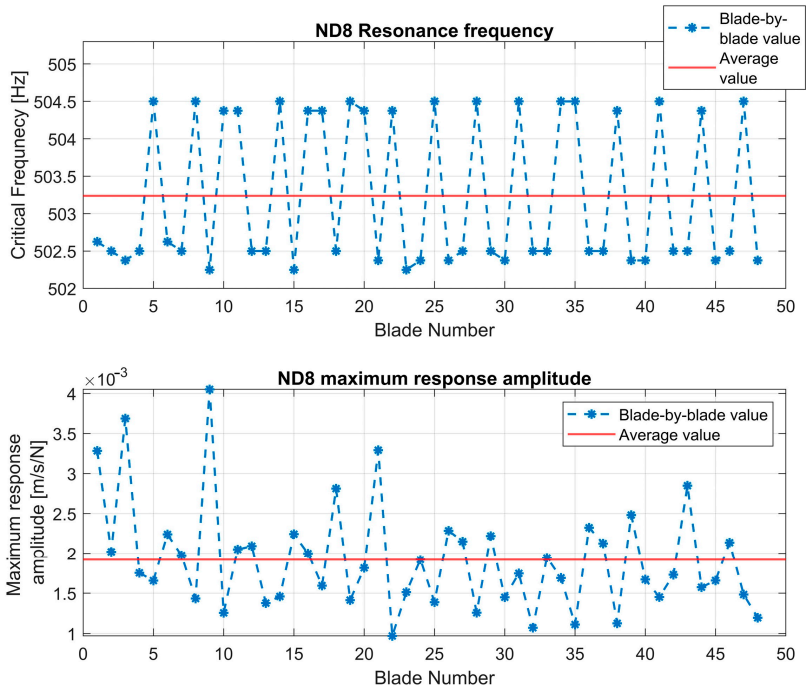

Figure 4. Critical frequency and maximum response for 3rd family ND8 mode.

It is clear from Figure 4 that the values identified for each blade are not the same. This happens due to the phenomenon called natural or intrinsic mistuning [24], which may occur due, for example, to manufacturing inaccuracies or assembly procedures. Therefore,

it is reasonable to summarize the results for all the blades with the mean value and standard deviation. These values are 503.2 and 1 Hz for the critical frequency and 1.9×10^{-3} and 6.7×10^{-4} m/s/N for the response.

2.2. Testing the Rotating Condition

2.2.1. Spinning Test Rig

For nonlinear responses measured in cases of friction damping caused by the action of UPDs, two 3D-printed Onyx retainer rings were designed to limit the UPDs' rotating motion to $+/-90^{\circ}$ from their nominal position in the cavity (Figure 5). These rings ensure proper UPD alignment, still allowing for translation and rotation within the cavity.

(**a**) (**b**)

Figure 5. (**a**) Shows 3D-printed retainer ring; (**b**) CAD drawing of spinning test rig.

2.2.2. Excitation System

Permanent magnets provide excitation to the system, since permanent rotating magnets are mounted at the tip of the blades in a repulsive configuration with respect to the static magnets on the flange, generating an excitation along axial direction. A piezoelectric load cell, which is applied to one of the non-rotating permanent magnets, is used to measure the force amplitude. The axial distance between the blades and permanent magnets can be regulated by the permanent magnet's screws in order to vary the amount of exciting force. Each magnet is affixed to the end of a screw, allowing for the adjustment of the axial gap relative to the disk blades. Six of these magnets are equipped with force transducers to measure the axial force applied to the blades during testing. The number of permanent magnets used for the test is directly linked to the engine order (EO) excitation in order to excite the desired mode under resonance conditions for a specific ND value.

2.2.3. Measurement System

The Blade Tip Timing (BTT) technique is used to measure blade response. The main principle behind the BTT technique is that, when a blade is rotating and vibrating, the Time of Arrival (ToA) of the blade tip next to the stationary sensor will be a function of the rotor speed and of the displacement due to its vibration [25]. By analyzing the ToA of each blade passing the sensor and the theoretical ToA of the non-vibrating blade, it is possible to evaluate the dynamic properties of each blade, i.e., the vibration amplitude, resonance frequencies, damping, engine order, number of nodal diameters, and the operating deflection shape [26].

The BTT system utilized in this research is a state-of-the-art system employing optical laser sensors. Five sensors were used for the direct detection of the blades' ToA in all tests and one additional sensor (1/rev sensor) was used to measure the rotational speed and serve as the standard for all other sensors.

In this research, a beam shutter configuration was employed for the Blade Tip Timing (BTT) method (Figure 6). This setup enhances measurement precision by accurately capturing blade tip passage, and reduces background noise interference, allowing the reliable and non-contact detection of tip dynamics [26].

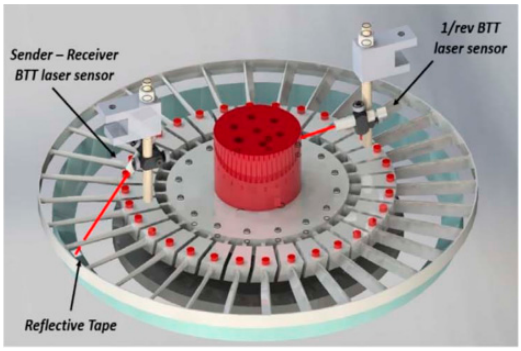

Figure 6. Beam shutter configuration.

2.2.4. Data Post-Processing

All the experimental data have been post-processed by using the Circumferential Fourier Fit (CFF) fitting method [27]. This method starts with the definition of the EO corresponding to the response and then fits all the vibration data with a sinusoidal wave for each average rpm value. The equation of the blade motion identified by the k-th sensor is as follows:

$$x_k(\omega) = c(\omega) + A(\omega) \cdot (\sin(EO \cdot 2\pi ft) \cdot \cos(\phi(\omega)) + \cos(EO \cdot 2\pi ft) \cdot \sin(\phi(\omega))) \quad (1)$$

where $A(\omega)$ and $\phi(\omega)$ are the amplitude and phase at a certain frequency and $c(\omega)$ is the blade's static position. For a given blade at each frequency, the displacement $x_k(\omega)$ is measured by each sensor. Equation (1) is applied individually for each sensor, and terms $A(\omega)$, $\phi(\omega)$, and $c(\omega)$ are determined through a least squares method, particularly if more than three sensors are utilized for measurements. Subsequently, the amplitude $A(\omega)$ can be plotted versus the rotational speed, as is demonstrated later.

3. Experimental Results

The experimental tests performed as part of this research, in accordance with the designated setup and procedure, were carried out utilizing an EO = 8 synchronous excitation applied to the disk. The tests were conducted under the following configurations:

- A tuned bladed disk without UPDs during testing.
- A tuned bladed disk with aluminum UPDs.
- A tuned bladed disk with steel UPDs.

Each test was performed with both an increase and decrease in the angular velocity. This was conducted to verify the repeatability of the disk output response across various frequency values and to verify the possible presence of nonlinearity producing stiffening or softening effects of the resonance peak. The maximum response amplitude (μm, 0-peak) and the corresponding critical frequency (Hz) are plotted for each of the 48 disk blades in Figures 7 and 8.

From Figures 7 and 8, it is possible to note a range in the variability of the peak amplitude and critical frequency between the blades, which takes place due to the phenomenon of mistuning. Although all the blades are assumed to be identical during cyclic symmetry analysis, there are some inevitable differences between various sectors, regarding the errors in the assembly procedure, the malfunctioning tolerances, the inhomogeneity of the material, or any wear phenomena during operation. The following figure illustrates the variability between the measured quantities from each blade (Figure 9).

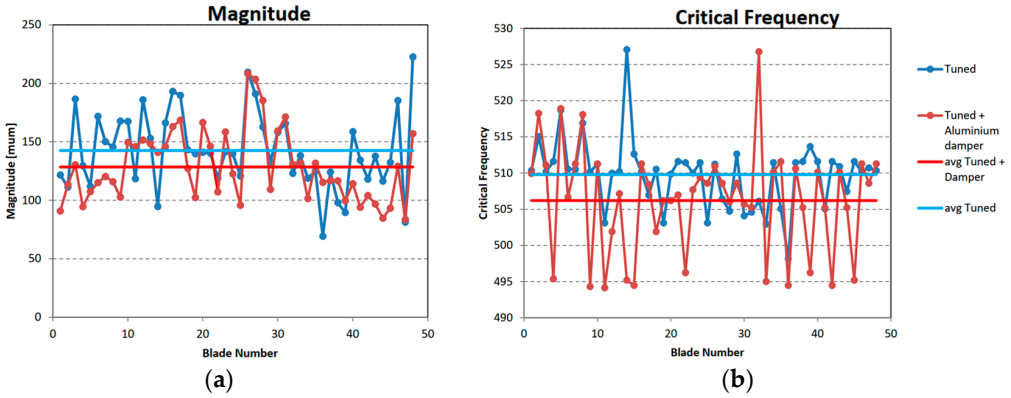

Figure 7. (**a**) The maximum response amplitude and (**b**) critical frequency for each of the 48 blades as well as the averaged one in tuned and tuned + aluminum UPD configurations.

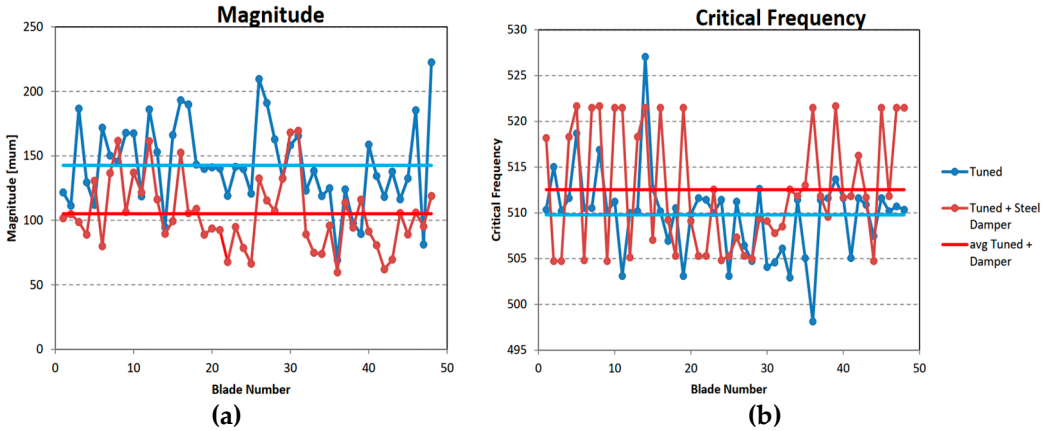

Figure 8. (**a**) The maximum response amplitude and (**b**) critical frequency for each of the 48 blades as well as the averaged one in tuned and tuned + steel UPD configurations.

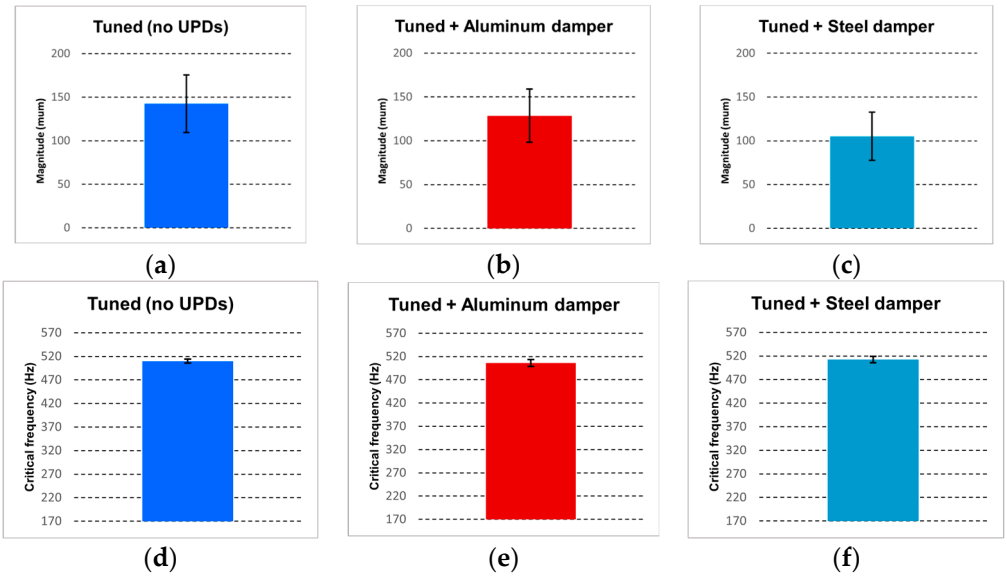

Figure 9. The average value and standard deviation of the maximum response amplitude for (**a**) tuned (no UPDs), (**b**) tuned + aluminum damper, and (**c**) tuned + steel damper configurations. The average value and standard deviation of the critical frequency for (**d**) tuned (no UPDs), (**e**) tuned + aluminum damper, and (**f**) tuned + steel damper configurations.

The numerical values are summarized in the following table (Table 1):

Table 1. The average value and standard deviation of the maximum response amplitude as well the critical frequency for different configurations.

Parameter	Configuration	Average Value	Standard Deviation
Maximum response amplitude	Tuned (no UPDs)	142.5 μm	33.1 μm
Maximum response amplitude	Tuned + aluminum damper	128.5 μm	30.4 μm
Maximum response amplitude	Tuned + steel damper	105.1 μm	27.6 μm
Critical frequency	Tuned (no UPDs)	509.8 Hz	4.6 Hz
Critical frequency	Tuned + aluminum damper	506.2 Hz	7.5 Hz
Critical frequency	Tuned + steel damper	512.5 Hz	6.6 Hz

As can be noticed from the results obtained, there is a slight increase in the critical frequency of the ND8 mode with respect to that obtained by modal hammer testing, specifically from 503.2 to 509.8 Hz. This phenomenon occurs due to centrifugal stiffening.

Furthermore, it is possible to evaluate the effectiveness of under-platform dampers (d) by comparing the average response amplitude in the presence of UPDs (A_{damp}) with respect to those in the nominally tuned configuration (A_{nom}).

$$d = \frac{A_{damp} - A_{nom}}{A_{nom}} 100 \tag{2}$$

The results obtained are as follows:

- Aluminum dampers: $d = 9.85\%$;
- Steel dampers: $d = 26.27\%$.

As anticipated from the preceding analysis, it is evident that the steel UPDs exhibit a greater damping capacity compared to the aluminum ones. This experimental damping will subsequently be used for a comparison against the corresponding percentage derived from the numerical analysis, aiming to estimate the accuracy of the simulated model relative to the actual case tested in the laboratory.

4. Numerical Analysis

The numerical simulations were carried out in Policontact software [28]. This simulation environment performs linear and nonlinear forced response analysis in the presence of friction contacts. The experimental post-processed data serve as an input for Policontact analysis since several parameters requested by the software are adjusted in order to match the experimental response.

Two different linear conditions can be calculated first:

- *Free response*: a linear forced response in the absence of UPDs, i.e., with no active friction contacts on the blade platforms.
- *Full-stick response:* a linear forced response in the presence of UPDs that are always in contact with the blade platform in a stick condition. Therefore, this configuration imposes higher stiffness and thus a higher critical frequency on the overall system.

The following input parameters are required by Policontact software to characterize the contact and determine the nonlinear forced response: the nodal diameter value, modal damping value, force amplitude, friction coefficient, number of nodes in contact (contact locations), and contact stiffnesses. The determination of each of them will be discussed individually in separate subsections.

4.1. Nodal Diameter

The nodal diameter under investigation was chosen to be ND-8 (third family) in order to meet the scaling criteria from the 144-blade disk. This was chosen in order to guarantee the same Inter-Blade Phase Angle (IBPA) of the reference disk.

4.2. Modal Damping Value

This value was determined by analyzing the experimental responses of individual blades without UPDs (free condition, reference 'linear' response). Ten responses were selected, focusing on those blades exhibiting a more consistent signal. These responses were then processed using a custom Matlab code designed for fitting the experimental curves with a Single-Degree-of-Freedom (SDOF) forced response. This code identifies the peak amplitude and corresponding frequency within a critical RPM range specified by the user. Subsequently, it generates a fitted curve with minimal deviation from the experimental data, utilizing the least squares criterion, while ensuring that the maximum amplitude and critical frequency remain consistent with the initial parameters. Using an average of the identified values, the modal damping ratio of the fitted curve will be set as the value in the Policontact software for the mode of interest.

The following formula represents the SDOF response to the harmonic excitations that are used for the fitting procedure:

$$A = \frac{A_{max} \cdot 2\,\xi}{\sqrt{\left(2\frac{\omega}{\omega_0}\xi\right)^2 + \left(1 - \left(\frac{\omega}{\omega_0}\right)^2\right)^2}} \tag{3}$$

Here, the following correspondences hold: A—Response amplitude, A_{max}—Peak amplitude, ξ—Modal damping, ω—Frequency of harmonic excitation, and ω_0—System natural frequency.

It is evident from the above formula that the only unknown parameter is ξ and thus it can be calculated. Figure 10 represents the output of the MATLAB code for one blade, where the blue curve represents the response of a generic blade that is fitted, with the red curve, defined as an SDOF forced response, characterized by the same peak amplitude and corresponding frequency value. The final value of modal damping is evaluated as the average of the estimated value identified on the 10 blades and set to 0.0032. This value is further used for simulations.

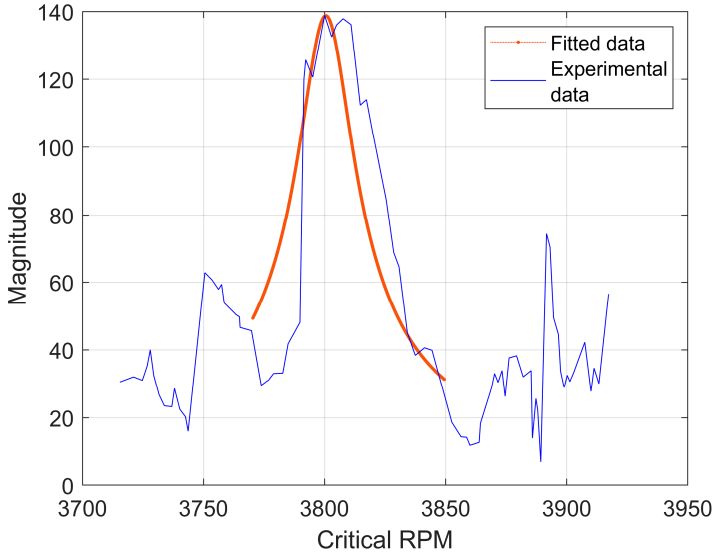

Figure 10. Example of one blade-response fit with an SDOF forced response.

4.3. Force Amplitude

As described in Section 2.2.2, the excitation force at the leading edge is applied at the blade tips by using permanent magnets. The magnitude of the force is inversely proportional to the square value of the air gap between the permanent magnet and blade tip. In order to obtain the numerical value of this force, which is further used in Policontact, a calibration procedure was undertaken in order to match the numerical peak amplitude in the free condition with the average blade response in the tuned configuration (no UPDs). This was made possible due to the linearity that characterizes this configuration. It was further verified that the recorded force signal measured by the load cell, after being processed by Fourier analysis to identify the EO-8 harmonic component, corresponds to the value set in Policontact.

Eventually, the magnitude of the force used for numerical simulations on EO8, for a 5 mm gap. was taken to be 0.27 N.

4.4. Friction Coefficient

A sensitivity analysis based on the variation of this parameter was conducted, using the following friction values as benchmarks: 0.2, 0.5, and 0.7. The comparison of nonlinear responses was performed while maintaining consistency with the contact nodes between the damper and the blade platform (specifically, contact locations 1, 2, and 3, as described below). It was observed that the damping capability increases with higher values of the friction coefficient. For our examination, a friction coefficient of 0.2 was chosen, as it best matches with the experimental response. This choice is also confirmed by theory [29,30], as the UPDs were subjected to a relatively low number of cycles during our experimental tests.

4.5. Contact Locations

During the experimental campaign, using the same test rig, a thorough visual examination of all 48 contact surfaces of the UPDs was conducted to assess any indications of wear. This analysis revealed the presence of eight common contact locations, as illustrated in Figure 11.

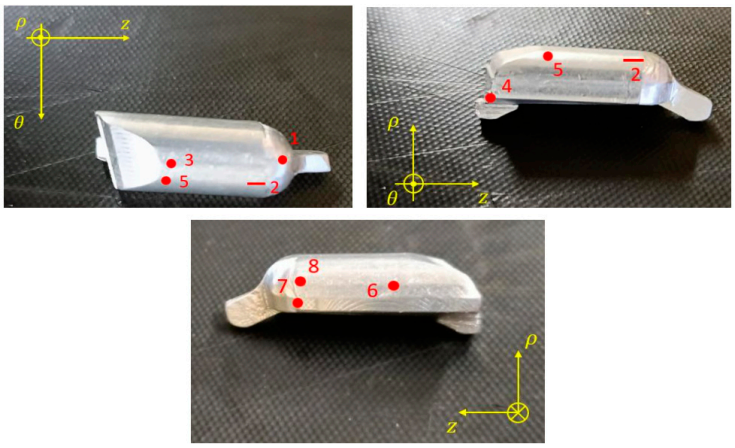

Figure 11. Eight common contact locations on the aluminum UPDs, identified after a visual inspection of all the 48 dampers.

Aluminum UPDs were chosen for the visual inspection since they exhibit a lower elastic modulus and thus make it easier to find the wear marks. The most common contact locations were observed to be 1, 2, and 3. The wear marks at these locations were found in 12, 47, and 17 of the 48 UPDs, respectively. Therefore, these contact locations were used in Policontact simulations both for aluminum and steel UPDs.

4.6. Contact Stiffnesses

To determine the tangential and normal stiffness values for both aluminum and steel dampers, the nonlinear peak amplitude obtained in Policontact was matched with the average experimental response in the presence of dampers. Specifically, a comparison was made between the scenario with all eight contact locations (Figure 11) and that with just the three most common ones, to assess the impact of this choice on contact stiffness values. The analysis revealed that varying the number of contact nodes did not significantly affect the contact stiffness values used to reconcile the numerical results with the experimental data.

Therefore, the contact stiffnesses set in Policontact are indicative of the overall contact and do not result in significant alterations in the nonlinear analysis. To better illustrate this, Figure 12 represents two nonlinear responses corresponding to eight and three contact locations for the steel damper. As can be seen, there is no major difference, except for a slight variation in the peak frequency value. However, as can be expected from the theory, a critical frequency corresponding to eight contact locations exhibits a larger value since it features more contact nodes, making it stiffer.

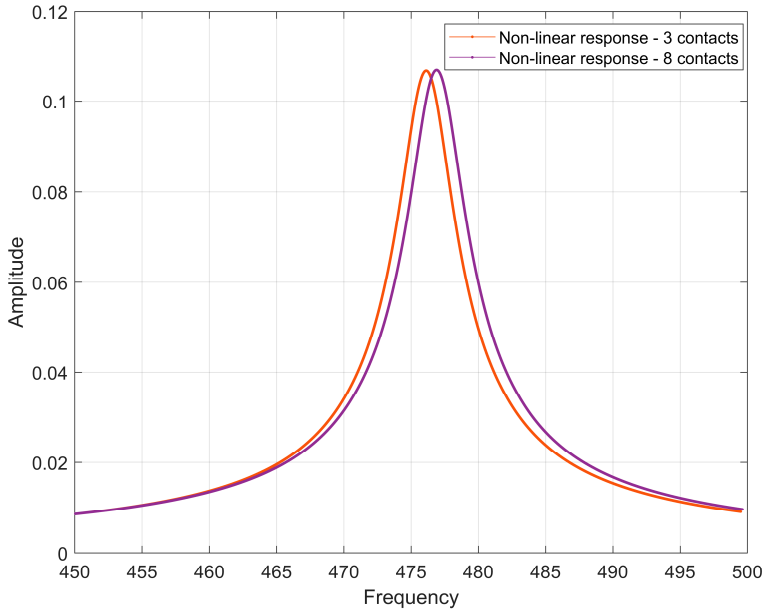

Figure 12. Nonlinear responses computed with 3 and 8 contact locations.

Eventually, by assuming the isotropic character of the material which imposes the same value both for horizontal and vertical stiffnesses, the 1000 N/mm and 3700 N/mm values are used for aluminum and steel UPDs. These values are not far from the ratio between the corresponding nominal Young moduli of the two materials.

4.7. Results

After the model update undertaken by means of the definition of all the necessary parameters required by the Policontact software, it is possible to simulate the nonlinear forced response in test conditions. Primarily, the linear analysis was performed for the nominally tuned configuration (without UPDs) in both free and full stick conditions (Figure 13). The full-stick condition is obtained by avoiding slipping in the contact model.

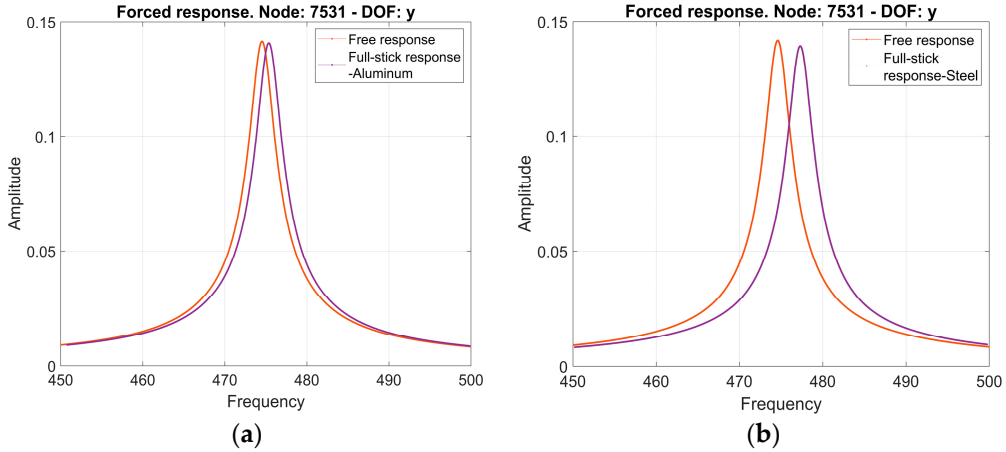

Figure 13. Linear forced response: Free and full-stick response with (**a**) aluminum damper and (**b**) steel damper.

The stiffening effect for the full-stick condition is evident from the figures above and is characterized by a greater critical frequency value and a slightly lower peak amplitude value. By keeping the same excitation amplitude, the nonlinear analysis was performed (Figure 14). The reference values used for all of the analysis to assess the damping performance of the UPDs were the free maximum amplitude and the corresponding peak frequency, numerically equal to 0.1419 mm and 474.6 Hz, respectively.

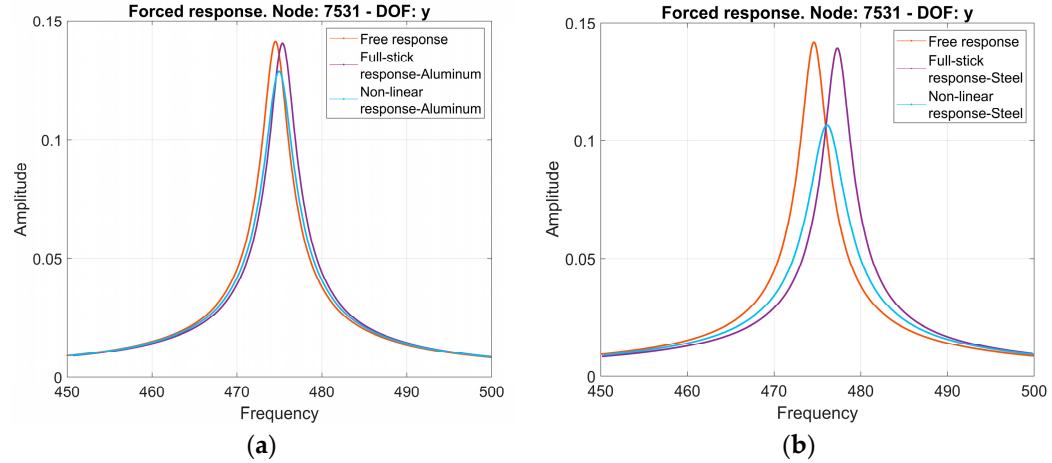

Figure 14. Linear and nonlinear forced responses of the tuned plus (**a**) aluminum UPD and (**b**) steel UPD configuration (ND8, 3rd modal family).

5. Comparison of Experimental and Numerical Results: Model Validation

The comparison was made for three main parameters of interest, namely, peak amplitude, critical frequency, and damping efficiency. Damping efficiency d was defined in the same way as in Equation (2).

The comparative analysis was performed on all of the three configurations studied herein: (a) nominally tuned (no UPDs), (b) tuned with aluminum UPDs, and (c) tuned with steel UPDs. The Tables 2–4 summarize the comparative analysis and indicates the discrepancies between numerical and experimental data.

Table 2. Experimental–numerical comparison for nominally tuned (no-UPD) configuration.

	Peak Amplitude (μm)	Critical Frequency (Hz)	Damping Efficiency (%)
Experimental	142.5	509.8	-
Numerical	141.9	474.6	-
Difference	*0.46%*	*6.9%*	-

Table 3. Experimental–numerical comparison for tuned + aluminum configuration.

	Peak Amplitude (μm)	Critical Frequency (Hz)	Damping Efficiency (%)
Experimental	128.5	506.2	9.85
Numerical	129.1	475	9.02
Difference	*−0.45%*	*6.16%*	*8.43%*

Table 4. Experimental–numerical comparison for tuned + steel configuration.

	Peak Amplitude (μm)	Critical Frequency (Hz)	Damping Efficiency (%)
Experimental	105.1	512.5	26.27
Numerical	106.8	476.1	24.74
Difference	*−1.61%*	*7.11%*	*5.82%*

From the results obtained, we can conclude of a strong correlation between the experimental and numerical data. This is further supported by the modulus of differences, which was always less than the minimum acceptable level of 10%. This makes us conclude that the numerical model accurately reproduces the real bladed disk average behavior.

Moreover, we can notice the greater damping capability of the steel UPDs with respect to the aluminum ones, which exhibit a 26% amplitude reduction.

6. Conclusions

In this paper, the nonlinear vibration analysis of an LPT bladed disk was carried out by considering different configurations, namely ones which were nominally tuned, tuned with aluminum dampers, and tuned with steel dampers. The nominally tuned configuration refers to the use of an array of nominally equal blades. The effectiveness of the damping capability of each configuration was studied as well. Primarily, the experimental activity was carried out on a test rig for a redesigned 48-blade disk which served as a surrogate for the original 144-bladed disk by taking into account all the necessary scaling criteria. The BTT system was used to measure the blade response. The system response and critical frequency were obtained for each of the 48 blades which exhibited a certain range of variability due to natural mistuning. Average values were taken for further consideration. The results obtained from the experimental test bring us to the conclusion that the predominant influence on the mistuning pattern arises from natural mistuning, rather than the presence of under-platform dampers. This finding underscores the significant role of inherent manufacturing and assembly variations in the dynamic response, highlighting that UPDs contribute less to mistuning than initially anticipated.

In the next section, a numerical analysis was performed with the Policontact software, which in our case required some system parameters to be taken from the experimental data. Finally, the comparison between the experimental and numerical results was carried out by evaluating the percentage difference among them. The percentage error in all the parameters and configurations did not exceed the minimum acceptable level of 10%. This, in turn, proves the reliability of our model and numerical results.

The minimum percentage error was observed for peak amplitude values rather than for the critical frequency or damping efficiency, not exceeding 2% for all the configurations.

The numerical model showed a good level of prediction for critical frequency and damping efficiency as well. Error differences of 6.9%, 6.16%, and 7.11% for critical frequency, as well as 8.43% and 5.82% for damping efficiency, in the cases of nominally tuned (no

UPDs), tuned + aluminum UPDs, and tuned + steel UPDs were obtained as a result of experimental–numerical result comparison.

The best damping capability can be seen for steel dampers, the damping efficiency for which stands at the level of 26.27%, which is almost 2.7 times more than for aluminum ones. This result can be related to the higher steel density which in turn imposes a higher normal static preload, resulting in more energy dissipation due to friction.

The novelty of this work lies in its innovative combination of experimental and numerical approaches to analyze the nonlinear vibrations of bladed disks. By integrating Blade Tip Timing (BTT) measurements with Policontact software simulations, this study provides a robust framework for validating the dynamic behavior of bladed disks. Additionally, the work distinguishes between intrinsic mistuning, caused by manufacturing and assembly variations, and contact mistuning introduced by under-platform dampers (UPDs), offering deeper insights into their respective effects on vibration response. Moreover, this research presents a 48-bladed example, scaled from a 144-bladed disk, enabling efficient dynamic analysis, repeatable testing, and the thorough inspection of under-platform dampers. Furthermore, the material-specific analysis comparing aluminum and steel UPDs reveals that steel demonstrates a significantly higher damping efficiency, attributed to its greater density and preload. This bring us to the conclusion that the normal preload has a very important effect on the determination of the final response of the bladed disk.

Looking ahead, future studies will concentrate on conducting repeatability tests to validate the accuracy of the experimental data. Additionally, a more comprehensive sensitivity analysis could be conducted on the contact points between the damper and the blade under the platform to gain deeper insights into their impact on response values.

Author Contributions: Conceptualization, G.B. and C.M.F.; methodology, M.C. and G.B.; software, G.B.; validation, E.R., A.G.D. and M.C.; formal analysis, M.C. and G.B.; investigation, M.C.; resources, E.R. and A.G.D.; data curation, G.B. and M.C.; writing—original draft preparation, U.U.; writing—review and editing, U.U. and C.M.F.; visualization, U.U. and G.B.; supervision, C.M.F. and G.B.; project administration, E.R. and A.G.D.; funding acquisition, C.M.F. and G.B. All authors have read and agreed to the published version of the manuscript.

Funding: This research effort was funded by the European Commission under the Horizon 2020 Program (grant agreement number 769346, project ARIAS—Advanced Research Into Aeromechanical Solutions, DOI: https://doi.org/10.3030/769346) [23].

Data Availability Statement: The original contributions presented in this study are included in the article. Further inquiries can be directed to the corresponding author(s).

Conflicts of Interest: Author Marta Conte, Emanuele Rosso, and Antonio Giuseppe D'Ettole are employed by the company Avio Aero. The remaining authors declare that the research was conducted in the absence of any commercial or financial relationships that could be construed as a potential conflict of interest.

References

1. Gastaldi, C. Vibration Control and Mitigation in Turbomachinery. Ph.D. Thesis, Politecnico di Torino, Turin, Italy, 2017.
2. Laxalde, D.; Thouverez, F.; Lombard, J.P. Forced response analysis of integrally bladed disks with friction ring dampers. *J. Vib. Acoust.* **2010**, *132*, 011013. [CrossRef]
3. Lupini, A.; Epureanu, B.I. A friction-enhanced tuned ring damper for bladed disks. *J. Eng. Gas Turbines Power* **2021**, *143*, 011002. [CrossRef]
4. Wu, Y.G.; Li, L.; Fan, Y.; Zucca, S.; Gastaldi, C.; Ma, H.Y. Design of dry friction and piezoelectric hybrid ring dampers for integrally bladed disks based on complex nonlinear modes. *Comput. Struct.* **2020**, *233*, 106237. [CrossRef]
5. Weihan, T.; Epureanu, B.I. Nonlinear dynamics of mistuned bladed disks with ring dampers. *Int. J. Non-Linear Mech.* **2017**, *97*, 30–40. [CrossRef]
6. Sun, Y.; Yuan, J.; Denimal, E.; Salles, L. Nonlinear Modal Analysis of Frictional Ring Damper for Compressor Blisk. *J. Eng. Gas Turbines Power* **2021**, *143*, 031008. [CrossRef]
7. Lupini, A.; Mitra, M.; Epureanu, B.I. Application of Tuned Vibration Absorber Concept to Blisk Ring Dampers: A Nonlinear Study. *J. Eng. Gas Turbines Power* **2019**, *141*, 101016. [CrossRef]

8. Cimpuieru, M.; Kripfgans, A.D.; Kelly, S.T.; Epureanu, B.I. Impact-Enhanced Resonant Vibration Absorber for Turbomachinery Blisks. In Proceedings of the ASME Turbo Expo, London, UK, 25 June 2024.
9. Hartung, A.; Retze, U.; Hackenberg, H. Impulse Mistuning of Blades and Vanes. *J. Eng. Gas Turbines Power* **2017**, *139*, 072502. [CrossRef]
10. Wu, Y.G.; Li, L.; Fan, Y.; Ma, H.Y.; Wang, W.J.; Christen, J.-L.; Ichchou, M. Design of semi-active dry friction dampers for steady-state vibration: Sensitivity analysis and experimental studies. *J. Sound Vib.* **2019**, *459*, 114850. [CrossRef]
11. Gao, Q.; Fan, Y.; Zucca, S.; Wu, Y.G.; Li, L. How frictional heat affects the performance of under platform dampers: Interface temperature and dynamic behaviors. In Proceedings of the ASME Turbo Expo, London, UK, 25 June 2024.
12. Tufekci, M. Development and application of a high-fidelity numerical tool for dynamic analysis of bladed disc systems with under platform dampers in aircraft engine turbines. In Proceedings of the ASME Turbo Expo, London, UK, 25 June 2024.
13. Ferhatoglu, E.; Gastaldi, C.; Botto, D.; Zucca, S. An experimental and computational comparison of the dynamic response variability in a turbine blade with under-platform dampers. *Mech. Syst. Signal Process.* **2022**, *172*, 108987. [CrossRef]
14. Firrone, C.M.; Zucca, S. Modelling Friction Contacts in Structural Dynamics and Its Application to Turbine Bladed Disks. In *Numerical Analysis—Theory and Application*; Awrejcewicz, J., Ed.; IntechOpen: London, UK, 2011; Chapter 14; pp. 301–333. [CrossRef]
15. Charleux, D.; Gibert, C.; Thouverez, F.; Dupeux, J. Numerical and Experimental Study of Friction Damping Blade Attachments of Rotating Bladed Disks. *Int. J. Rotating Mach.* **2006**, *2006*, 071302. [CrossRef]
16. Denimal, E.; Wong, C.; Salles, L.; Pesaresi, L. On the Efficiency of a Conical Underplatform Damper for Turbines. *J. Eng. Gas Turbines Power* **2021**, *143*, 021020. [CrossRef]
17. Li, L.; Lu, B.; Xu, W.; Wang, C.; Wu, J.; Tan, D. Dynamic behaviors of multiphase vortex-induced vibration for hydropower energy conversion. *Energy* **2024**, *308*, 132897. [CrossRef]
18. Sever, I.A.; Petrov, E.P.; Ewins, D.J. Experimental and Numerical Investigation of Rotating Bladed Disk Forced Response Using Underplatform Friction Dampers. *J. Eng. Gas Turbines Power* **2008**, *130*, 042503. [CrossRef]
19. Botto, D.; Gastadi, C.; Gola, M.M.; Umer, M. An Experimental Investigation of the Dynamics of a Blade with Two Under-Platform Dampers. *J. Eng. Gas Turbines Power* **2018**, *140*, 032504. [CrossRef]
20. Gastaldi, C.; Gola, M. Testing, Simulating and Understanding Under-Platform Damper Dynamics. In Proceedings of the VII European Congress on Computational Methods in Applied Sciences and Engineering, Crete, Greece, 5–10 June 2016. [CrossRef]
21. Li, D.; Du, C.; Li, H.; Meng, G. Numerical and Experimental Study on Dummy Blade with Underplatform Damper. *Machines* **2024**, *12*, 461. [CrossRef]
22. Fantetti, A.; Setchfield, R.; Schwingshackl, C. Nonlinear dynamics of turbine bladed disk with friction dampers: Experiment and simulation. *Int. J. Mech. Sci.* **2023**, *257*, 108510. [CrossRef]
23. ARIAS (Advanced Research Into Aeromechanical Solutions). Research Project Funded by European Union's Horizon 2020 Research and Innovation Programme Under Grant Agreement № 769346. Available online: https://www.arias-project.eu/ (accessed on 9 October 2024).
24. Feiner, D.M.; Griffin, J.H. Mistuning identification of bladed disks using a fundamental mistuning model—Part I: Theory. *J. Turbomach.* **2002**, *124*, 597–605. [CrossRef]
25. Zielinski, M.; Ziller, G. Noncontact Blade Vibration Measurement System for Aero Engine Application. MTE Aero Engines GmbH, ISABE-2005-1220. 2005. Available online: https://api.semanticscholar.org/CorpusID:114618803 (accessed on 9 October 2024).
26. Battiato, G.; Firrone, C.M.; Berruti, T.M. Forced response of rotating bladed disks: Blade Tip-Timing measurements. *Mech. Syst. Signal Process.* **2017**, *85*, 912–926. [CrossRef]
27. Hood Technology. *Analyze Blade Vibration User Manual, version 7.5*; Hood Technology: Hood River, OR, USA, 2014.
28. Firrone, C.M.; Battiato, G. A Reliable Pre-Processing for the Simulation of Friction Joints in Turbomachineries and Its Validation: A Case Study with Policontact. In Proceedings of the ASME Turbo Expo 2019: Turbomachinery Technical Conference and Exposition, Volume 7B: Structures and Dynamics, Phoenix, AZ, USA, 17–21 June 2019. [CrossRef]
29. Fantetti, A.; Botto, D.; Zucca, S.; Schwingshackl, C. Guidelines to use input contact parameters for nonlinear dynamic analysis of jointed structures: Results of a round robin test. *Tribol. Int.* **2024**, *191*, 109158. [CrossRef]
30. Lavella, M.; Botto, D. Fretting wear damage mechanism of CoMoCrSi coatings. *Wear* **2021**, *477*, 203896. [CrossRef]